Corrosion of AISI 316L Stainless Steel Pipe in a Complex Ammoniacal Medium

Felipe de Aquino Lima(✉), Ana Paula Neiva de Moura Santos, and Dalila Moreira da Silveira

Department of Chemical Engineering, Federal University of São João del Rei, Ouro Branco, Brazil
dalilams@ufsj.edu.br

Abstract. AISI 316L stainless steels are widely used in industrial pipes due to their resistance to corrosion and oxidation. However, some medium may favor incrustation and corrosion. In this scenario, the objective of the present research was to evaluate the deterioration of an AISI 316L steel tube for 12 months of industrial use. The medium contains 26,8011.00 mg/L of phosphate, 9,457.00 mg/L of chloride, 6.69 mg/L of sulfide, 6.08 mg/L of ammonia, and 1.88 mg/L of cyanide at a temperature of 200 °C and pressure of 12 kg/cm^2. After the period of industrial use, the tube was analyzed by scanning electron microscopy, dispersive energy spectroscopy, and optical microscopy. The chemical composition of the incrustation on the tube surface was verified by X-ray diffraction and X-ray fluorescence spectrometry. It was verified that sulfur compounds, such as sulfide, were the main corrosive agents on the tube, and cyanide accelerated this process. The medium's characteristics, such as the presence of chloride and phosphate salts, temperature, and pH (5.05), increased the corrosion rate on the tube, consuming about 30 cm of its length. It was observed the occurrence of stress corrosion, added to these compounds, caused sensitization of the material and weakening of metallic bonding.

Keywords: Corrosion · Tube · Distillation · Ammonia · Incrustation

1 Introduction

In the industrial project implementation, pipe costs represent, on average, 20% of the total cost of installation and 45% of the equipment costs. In this scenario, the industry faces the challenge of the choice of piping material, since this material must be resistant to the operational conditions and the environment they will be submitted to guarantee the mechanical integrity of the pipes and the feasibility of this application [1].

Austenitic stainless steels, such as AISI 316L, are widely used in industrial plants due to their excellent resistance to corrosive process at low temperatures and high resistance to oxidation and fatigue at high temperatures. However, its low hardness and low wear resistance can limit these applications [2–4].

Therefore, it is necessary to evaluate the process's operating conditions, such as temperature, pressure, and chemical compounds present in the medium, before deciding

Y. Iano et al. (Eds.): BTSym 2020, SIST 233, pp. 617–626, 2021.
https://doi.org/10.1007/978-3-030-75680-2_68

to use this type of steel. Some authors identified that the presence of compounds such as sulfides and chlorides, associated with temperatures in the range of 60 to 90 °C caused corrosion failure in AISI 316 L steel tube [5].

In a treatment plant of coke oven gas, the most aggressive compounds to the pipes are impurities, such as ammonia, sulfide, cyanide, and chloride [6]. In some parts of the process, when the concentration of these gases increases, the medium is more susceptible to corrosion.

During the treatment of coke oven gas, it is possible to selectively absorb ammonia using phosphoric acid and to distill this solution to obtain anhydrous ammonia. This product is intended for the production of dyes, pharmaceutical products, naphthalene, insecticides, also destined for the leather and concrete industry [7, 8].

Dias and collaborators [9] studied the corrosion in three types of stainless steels (AISI 304, 316 L e 321) used in a steelmaking process. Electrolytic tests were carried out using ammonia liquor and a chloride solution containing 2.5% (w/w) of NaCl. The electrolytic tests showed that the presence of molybdenum in the chemical composition of AISI 316 L steel did not affect the resistance to the corrosive action of the medium, being evidenced in the NaCl tests.

In another study about the corrosion in the heat-affected zone (HAZ) of AISI 316L stainless steel, caused by heavy crude oil, the samples heat-treated at 200 °C and 300 °C showed corrosion by iron sulfide products. This shows that media containing sulfide at this temperature can induce corrosion in this type of steel [10].

The presence of cyanide in the medium intensifies the corrosion process. This compound reacts with the iron sulfide and exposes the metal surface, leaving it unprotected and susceptible to a new corrosive attack. The iron oxides present in the medium reacts with the formed ferrocyanide complex and produces ferric ferrocyanide, which shows intense blue coloration, easily identified [11].

Thus, although there are studies that evaluate the resistance of stainless steels in various media [12–17], the evaluation under real operating conditions needs to be explored. In this scenario, this work aimed to study the corrosion mechanism and its products that affect the tube used in a distillation column of ammonia and phosphoric acid in a real industry.

2 Materials and Methods

2.1 Tube and Medium Characteristics

The tube used in this work was allocated in a real steel industry for 12 months, specifically in a distillation column to recover ammonia and phosphoric acid from an ammonia absorber, according to the schematic representation in Fig. 1. The operating pressure of the column was 12 kg/cm^2. The chemical composition of the steel before the operation is shown in Table 1. Table 2 shows the chemical composition of the medium in which the tube was submerged at a temperature of 200 °C. The characterization followed the methodology available in the Standard Methods for the Examination of Water and Wastewater [18].

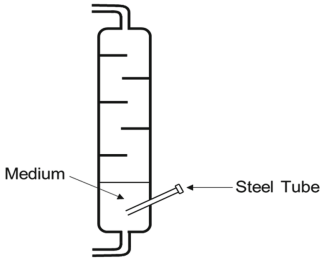

Fig. 1. Schematic representation of the distillation column showing the location of the tube.

Table 1. Nominal chemical composition of AISI 316L stainless steel before the use

Elements	C	Mn	Si	P	S	Cr	Ni	Mo	HV	HB
wt (%)	0.03	2.00	0.75	0.045	0.030	17.00	14.00	3.00	185	200

Table 2. Chemical composition of the medium in which the tube was submerged

Parameter	Unit	Method [12]	Concentration (mg/L)
Total ammonia	mg/L	4500 - B	6.08
Cyanide	mg/L	4500 CN^- - D	1.88
Calcium Hardness	mg/L	3500 Ca^- - B	5.18
Phenol	mg/L	5530 - C	1.43
Total iron	mg/L	3500 Fe iron - B	52.00
Oils and greases	mg/L	5520 - D	67.20
pH	–	4500	5.05
Total sulfur	mg/L	4500 - E	0.10
Silicon Dioxide	mg/L	4500 - C	12.00
Suspended solids	mg/L	2540 - B	215.00
Sulfide	mg/L	4500 - B	6.69
Chloride	mg/L	4500 Cl^- - D	9,457.00
Phosphate	mg/L	4500 P - C	26,8011.00

2.2 Analysis of AISI 316L Stainless Steel Tube

After 12 months of industrial use, tube samples were submitted to analysis of Optical Microscopy and Scanning Electron Microscopy (SEM) coupled to the Spectroscopy System Energy Scattering X-rays (EDS). The micrographs were obtained using a Clamex Optical Microscope. SEM/EDS analyses were carried out using a Quanta 400 FEI microscope equipped with an EDS system Bruker XFlash 4030, and the magnification used

was 120x. Tube samples without incrustations were submitted to Vickers Microhardness (HV) and Brinell Microhardness (HB) analyses according to ASTM A370 [19] and as chemical composition by X-Ray Fluorescence Spectrometry (Shimadzu XRF 1800 spectrometer).

2.3 Corrosion Deposits Analysis

Corrosion deposits were removed from the tube surface and analyzed by X-ray diffraction (XRD) and X-Ray Fluorescence Spectrometry (XRF) to quantify inorganic compounds. The XRD analysis was carried out in a Rigaku diffractometer (Miniflex 600) operating with CuKα rad radiation by the powder method. The goniometer velocity was 2°/min to detect the crystalline phase at a range between 5° and 80° (2θ). For XRF analysis, the sample was oven-dried and calcined at 875 °C for 4 h. After calcination, the sample was fused with potassium carbonate, digested with hydrochloric acid, and then analyzed on a Shimadzu XRF 1800 spectrometer.

3 Results and Discussion

This work used an AISI 316L stainless steel tube in a steam pipe from a distillation process to recover ammonia and phosphoric acid. Figure 2 shows the tube before and after its installation in the real process.

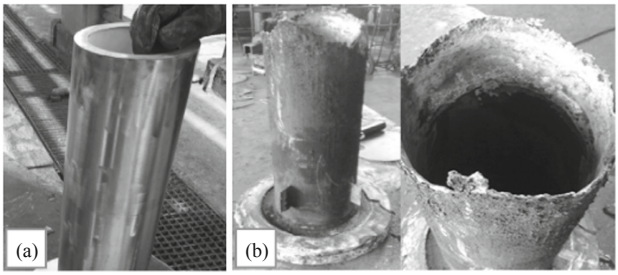

Fig. 2. AISI 316L stainless steel tube (a) new (b) after 12 months of industrial use.

Figure 2(b) displays the visual aspect of the tube, showing that the tube was deteriorated when compared with the new one (Fig. 2(a)). It can be seen that the length of the tube was reduced around 30 cm due to the exposition of ammonia, cyanide, sulfide, and chloride in an acid medium (pH of 5.05) subjected to high pressures and temperatures.

Table 3 shows the chemical composition of steel and Vickers and Brinell Microhardness analysis after 12 months of industrial use. The analysis of Microhardness resulted in the same value, 165 HV, HB, different from its nominal value given in Materials and Methods. According to ABNT NBR-5601, the maximum value for this steel type is 217 HV [20], showing that the corrosive process did not significantly affect this parameter.

Changes in composition in relation to the nominal values of the new tube were observed. As AISI 316L austenitic stainless steel contains molybdenum, Rokosz and

Table 3. Chemical composition of AISI 316L stainless steel after 12 months of industrial use.

Elements	C	Mn	Si	P	S	Cr	Ni	Mo	HV	HB
wt (%)	0.02	1.40	0.56	0.035	0.003	16.86	10.23	2.03	165	165

collaborators [17] demonstrated that in the presence of phosphate and sulfate medium, a stable surface layer of iron, chromium, and molybdenum compounds is formed. However, a very corrosive medium can access the entire thickness of the material, damaging it. The decrease in carbon (from 0.03 to 0.02%), molybdenum (from 3.00 to 2.03%), and chromium (17.00 to 16.86%) in samples after industrial use in relation to the initial values can be associated with the formation of this passive layer, which due to the corrosivity of the medium was not enough to prevent degradation of the pipe.

Figure 3 shows the electronic images of the most deteriorated region of the tube obtained by SEM. In the demarcated area, in Fig. 3(a), the crack propagation can be observed due to the sensitization of steel by the corrosive environment, such as by sulfides and chlorides, together with the high pressure of the steam and the distillation column [12, 13]. Table 4 presents the semiquantitative analysis of the spectra obtained by EDS of the areas numbered in Fig. 3(b), through which it was possible to identify the presence of corrosion product consisting basically of oxygen (O), phosphorus (P), and sulfur (S) elements.

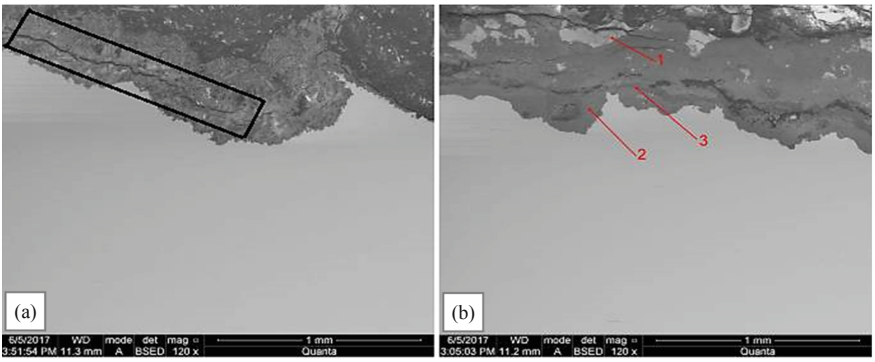

Fig. 3. Electronic image with an approximation of 120x of the most deteriorated region (tip) presents in the tube, where (a) shows the demarcated area of crack propagation and (b) shows the points where spectra were obtained by EDS.

Table 4. Semiquantitative medium chemical composition obtained by EDS.

Elements	O	P	Ni	Cr	Fe	S	Ca	Mn
wt (%)	37.12	24.68	10.91	10.66	10.31	5.64	0.56	0.13

The micrograph of the tube, presented in Fig. 4, showed that the basic structure is constituted by austenitic matrix and little occurrence of ferrite. There were no structural abnormalities that could be associated with the tube corrosion; nonetheless, it is observed that the operating conditions to which the tube was submitted may have weakened this region. The small change in nickel and manganese content in Table 3 corroborates these data, as this material plays an important role in the stability of the austenitic structure at high temperatures [21–23].

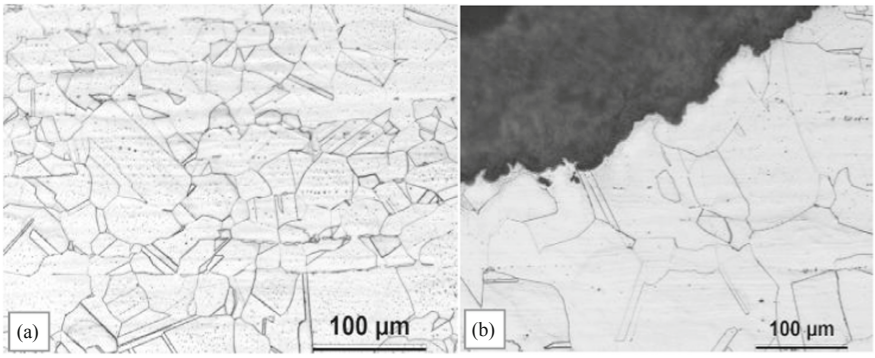

Fig. 4. Micrograph of the tube after 12 months of industrial use, where (a) shows the basic structure present in the tube sample and (b) shows the microstructure in the corrosion region.

Figure 3 and 4 showed that the structure of the tip of the tube deteriorated. These images showed how intense the degradation of stainless steel was due to the contact with the compounds of sulfides, chlorides, cyanides, phosphates, and ammonia. It is observed that the material has a generalized corrosion, with many cracks and deformations on the exposed surface.

The composition of the incrustations was confirmed in XRD and XRF. The diffractogram is shown in Fig. 5, and the chemical composition of XRF is shown in Table 5. X-ray diffractogram of the corrosion deposits collected from the tube surface shown in Fig. 5 pictures the presence of characteristic peaks of ferric ferrocyanide (17.37°, 24.71°, and 35.16°), that responsible for the Prussian blue pigment found on the tube surface; of Pyrite FeS_2 (28.96°) and hematite Fe_2O_3 (36.04°). The presence of ferric ferrocyanide shows the influence of the cyanide ion on the corrosion process and in the deposit formation, since the Prussian blue coloration was also found in regions less deteriorated by corrosion [24]. The presence of hematite was also verified by XRF, as presented in Table 5, corroborating with the XDR analysis. As presented in Table 5 and Fig. 5, it was possible to verify that the column's operating temperature favored the formation of hematite in relation to other oxides, such as magnetite and goethite, probably due to the reactions occurring between the stainless steel and the compounds present in the column.

The identification of other oxides in the XRF analyses, which were not previously identified by XRD, is due to the sample's preparation, since, in the XRF analyses, it

was previously calcined, which caused the elimination of organic compounds and the obtaining the oxide phase.

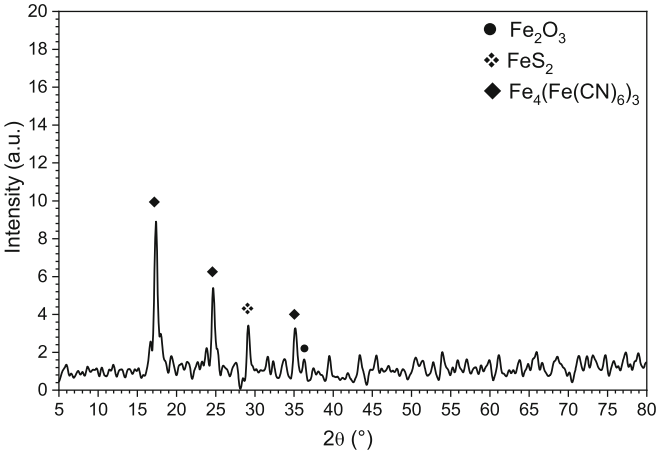

Fig. 5. X-ray Diffractogram of the tube incrustations after 12 months of industrial use.

Table 5. Medium chemical composition of deposits collected from the tube surface.

Oxide (%)	P_2O_5	Fe_2O_3	Na_2O	SiO_2	MgO
	59.27	43.52	6.28	0.74	0.25

The data obtained with the XRD and XRF corroborate with an increase in the composition of sulfur, phosphorus, and oxygen obtained by the EDS analyses. Also, the composition of the incrustations contains compounds that were possibly formed by contact with the medium, occurring reactions that led to the appearance of elements of the medium that were not previously found in the tube. The presence of sulfide compounds in the medium is aggressive due to their reduction to H2S, which is indicated as the main corrosion agent by sulfation [25]. This process is intensified in temperatures between 200 and 500 °C. The reaction of this compound with the tube surface can favor the increase of the corrosion rate through the formation of a sulfide layer. The free cyanide present in the medium can destabilize this layer, while sulfur inhibits the reaction of recombination of molecular hydrogen, allowing its permeation in the steel's crystal lattice [26–28].

Two effects can be observed when occurs the hydrogen permeation in the metal structure and their accumulation in the sites of the crystal lattice: the sensitization of the mechanical properties and the weakening of the metallic bonds, followed by the cracks nucleation, which can be accelerated in the presence of cyanide [29, 30].

The joint action of the stresses caused by the fluid at this operating pressure and the medium's composition may have conditioned stress corrosion and wakening by hydrogen. In the tube shows in Fig. 6, it is possible to observe that the deterioration

intensity was greater in the area near the point that was completely submerged in the medium, as identified by the arrow.

Fig. 6. Visual analyses of the tube with the arrow indicating the direction of the steam flow.

It was possible to see that the stainless steel in the presence of corrosive compounds in a distillation column influenced the corrosion process, in which the reactions generated their bluish and greenish appearance. These reactions were influenced by the high temperature and pressure that the tube was put through. The use of this material in these conditions is not indicated, mainly due to the constant changes that must be carried out, exposing people to the risk of coming into contact with this distillation tower's contents, such as ammonia and phosphoric acid.

As a suggestion to future work, it is interesting to explore ways to increase the useful life of steam injection tubes inserted in corrosive media, such as other types of materials or metal coatings to protect the material. It should also be used a higher number of samples to obtain more statistically significant results.

4 Conclusions

The corrosion process in AISI 316L stainless steel tube was evaluated and associated with the occurrence of stress corrosion and hydrogen weakening. In summary, it was observed that in a real process, the main cause of corrosion was due to the high operating pressure, temperature, and the presence of sulfides, phosphates, and cyanides in the medium. The composition of the corrosion products was mainly phosphorus, oxygen, and sulfur. The presence of cyanide intensifies the corrosion process and led to the formation of ferric ferrocyanide, a compound associated with Prussian blue coloration observed. In this context, this work aims to contribute to the industrial field, showing that the AISI 316L stainless steel can be a corrosion target in the distillation column of ammonia. In the end, further works can be developed by exploring ways to avoid the corrosive process to diminish costs with equipment in the industry.

References

1. Telles PCS (2012) Tubulações Industriais: Materiais, Projetos e Montagem. Editora LTC, Rio de Janeiro

2. Arifvianto B, Suyitno M (2012) Effects of surface mechanical attrition treatment (SMAT) on a rough surface of AISI 316L stainless steel. Appl Surface Sci 258:4538–4543
3. Li Y, Wang Z, Wang L (2014) Surface properties of nitrided layer on AISI 316L austenitic stainless steel produced by high temperature plasma nitriding in short time. Appl Surface Sci 298:243–250
4. Pham MS, Solenthaler C, Janssens KGF, Holdsworth SR (2011) Dislocation structure evolution and its effects on cyclic deformation response of AISI 316L stainless steel. Mater Sci Eng: A 528:3261–3269
5. Adair ST, Attwood PA (2014) In-service stress corrosion cracking of AISI 316L stainless steel in an H2S environment. Corros Eng Sci Technol 49:396–400
6. Vieira WP (2004) Estudo de corrosão em tubulações de gás de coqueria [Doctor thesis]. Federal University of Espírito Santo, Vitória
7. Busca G, Pistarino C (2003) Abatement of ammonia and amines from waste gases: a summary. J Loss Prev Process Ind 16:157–163
8. Ferreira OS (2019) Modelos de Negócios e Sustentabilidade Ambiental - a ecologia industrial na siderurgia no Brasil. Braz J Bus 1:669–681
9. Dias FMS, Oliveira AS, Carneiro FP, Cândido LC (2008) Estudo da corrosão de aços inoxidáveis do tipo AISI: 304, 316 L e 321 em meios amoniacais de uma usina siderúrgica empregando-se ensaios eletroquímicos. In: Proceedings of 63° Congresso Anual da ABM. Associação Brasileira de Metalurgia e Materiais, São Paulo, pp 2354–2361
10. Silva CC, Sant'ana HB, Farias JP (2009) Evaluation of AISI 316L stainless steel welded plates in heavy petroleum environment. Mater Des 30:1581–1587
11. Silva PR, Ponte HA, Ponte MJJS, Kaminari NMS (2011) Development of a new electrochemical methodology at carbon steel/Na_2S system for corrosion monitoring in oil refineries. J Appl Electrochem 41:317–320
12. Hsu JP, Wang D, Kahn H, Ernst F, Michal GM, Heuer AH (2013) Fatigue crack growth in interstitially hardened AISI 316L stainless steel. Int J Fatigue 47:100–105
13. Kim YH, Kim DG, Sung JH, Kim IS, Ko DE, Kang NH, Hong HU, Park JH, Lee HW (2001) Influences of Cr/Ni equivalent ratios of filler wires on pitting corrosion and ductility-dip cracking of AISI 316L weld metals. Met Mater Int 17:151–155
14. Ferreira EA, Noce RD, Fugivara CS, Benedetti AV (2013) Influence of ethanol, acidity and chloride concentration on the corrosion resistance of AISI 316L stainless steel. J Braz Chem Soc 24:397–405
15. Hoseinieh SM, Shahrabi T (2017) Influence of ionic species on scaling and corrosion performance of AISI 316L rotating disk electrodes in artificial seawater. Desalination 409:32–46
16. Mejía-Caballero I, Palomar-Pardavé M, Trinidad JM, Romero-Romo M, Pasten-Borja RP, Lartundo-Rojas L, López-García C, Campos-Silva I (2015) Corrosion behavior of AISI 316 L borided and non-borided steels immersed in a simulated body fluid solution. Surface Coat Technol 280:384–395
17. Rokosz K, Lahtinen J, Hryniewicz T, Rzadkiewicz S (2015) XPS depth profiling analysis of passive surface layers formed on austenitic AISI 304L and AISI 316L SS after high-current-density electropolishing. Surface Coat Technol 276:516–520
18. American Public Health Association (2012) Standard methods for examination of water and wastewater. Washington DC
19. American Society for Testing and Materials (2008) Standard Test Methods and Definitions for Mechanical Testing of Steel Products: A370. West Conshohocken (2008)
20. Associação Brasileira de Normas Técnicas (2011) NBR-5601: Aços inoxidáveis - Classificação por composição química. 2ª ed
21. Revie RW, Uhlig HH (2008) Corrosion and corrosion control. Wiley Interscience, Hoboken

22. Potgieter JH, Olubambi PA, Cornish L, Machio CN, Sherif ESM (2008) Influence of nickel additions on the corrosion behaviour of low nitrogen 22% Cr series duplex stainless steels. Corros Sci 50:2572–2579
23. Bautista A, Blanco G, Velasco F (2006) Corrosion behaviour of low-nickel austenitic stainless steels reinforcements: a comparative study in simulated pore solutions. Cem Concr Res 36:1922–1930
24. Cabrera-Sierra R, Sosa E, Oropeza MT, González I (2002) Electrochemical study on carbon steel corrosion process in alkaline sour media. Electrochimica Acta 47:2149–2158
25. Beidokhti B, Dolati A, Koukabi AH (2009) Effects of alloying elements and microstructure on the susceptibility of the welded HSLA steel to hydrogen-induced cracking and sulfide stress cracking. Mater Sci Eng A 507:167–173
26. Vieira MM, Gomes JACP, Baptista W, Joia CJBM (2002) Efeito do pH na corrosão e permeação de hidrogênio em aço carbono em presença de água ácida desaerada. In: Proceedings of 6° COTEQ - Conferência Sobre Tecnologia de Equipamentos & 22° CONBRASCORR - Congresso Brasileiro de Corrosão. Instituto Brasileiro de Petróleo, Gás e Biocombustíveis, Rio de Janeiro
27. Gentil V (2012) Corrosão, 6th edn. LTC, Rio de Janeiro
28. Jambo HCM, Fófano S (2009) Corrosão: Fundamentos, Monitoração e Controle. Ciência Moderna Ltda, Rio de Janeiro
29. Vianna CS, Chicot D, Lesage J, Miranda PEV (2004) Difusão do Hidrogênio em Martensita. Revista Matéria 9(1):01–11
30. Tiwari GP, Bose A, Chakravartty JK, Wadekar SL, Totlani MK, Arya RN, Fotedar RN (2000) A study of internal hydrogen embrittlement of steels. Mater Sci Eng A 286:269–281